Towards improving charge/discharge rate of latent heat thermal energy storage (LHTES) by embedding metal foams in phase change materials (PCMs)

Du, Yanping; Ding, Yulong

DOI:
10.1016/j.cep.2016.08.003

Document Version
Peer reviewed version

Citation for published version (Harvard):
Du, Y & Ding, Y 2016, 'Towards improving charge/discharge rate of latent heat thermal energy storage (LHTES) by embedding metal foams in phase change materials (PCMs)', Chemical Engineering and Processing, vol. 108, pp. 181-188. https://doi.org/10.1016/j.cep.2016.08.003

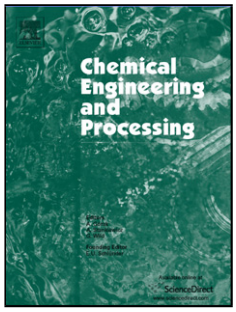

Title: Towards improving charge/discharge rate of latent heat thermal energy storage (LHTES) by embedding metal foams in phase change materials (PCMs)

Author: Yanping Du Yulong Ding

PII: S0255-2701(16)30263-X
DOI: http://dx.doi.org/doi:10.1016/j.cep.2016.08.003
Reference: CEP 6838

To appear in: *Chemical Engineering and Processing*

Received date: 7-4-2016
Revised date: 3-8-2016
Accepted date: 4-8-2016

Please cite this article as: Yanping Du, Yulong Ding, Towards improving charge/discharge rate of latent heat thermal energy storage (LHTES) by embedding metal foams in phase change materials (PCMs), Chemical Engineering and Processing http://dx.doi.org/10.1016/j.cep.2016.08.003

Towards improving charge/ discharge rate of latent heat thermal energy storage (LHTES) by embedding metal foams in phase change materials (PCMs)

Yanping Du[1,*] and Yulong Ding[2]

[1] *School of Chemical and Process Engineering, University of Leeds, LS2 9JT, UK*

[2] *School of Chemical Engineering, University of Birmingham, Edgbaston, Birmingham, B15 2TT, UK*

*Corresponding Author, email: Yanping.Du@csiro.au

Graphical abstract

By embedding Al foams in the PCMs, it was seen in Figure 9 that the excess temperature of paraffin-Al foams composite was smaller than $NaCO_3$–Al foams composite, indicating the former had bigger cold discharging rate under the same conditions. This is because paraffin-Al foams composite has the effective thermal diffusivity of $5.763\times10^{-6} m^2/s$, which is 42.5% higher than the value of the $NaCO_3$ –Al foams composite.

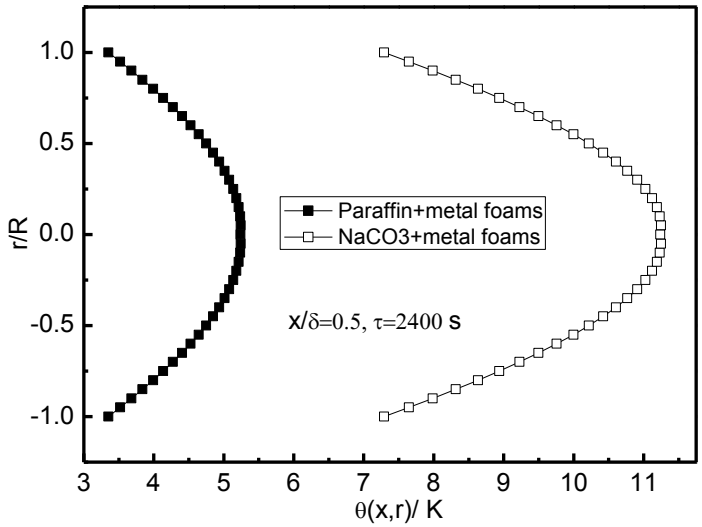

Highlights

PCM-metal foams composite is highly potential to be used as the storage medium;

· The product solution method was adopted to synthesize the analytical solutions;

· The cold discharge rate of the composite materials was enhanced by approximately 8 times;

· The value of effective thermal diffusivity was proved in weighing the charge/ discharge rate.

Abstract: PCMs-metal foams composite has been used in LHTES for improving the charge/ discharge rate of the system. Due to the high exergy efficiency of cold energy storage (CES) systems, cold charging/ discharging behaviours of the PCM-metal foams composite in CES

was particularly analysed. The product solution method was adopted to synthesize the analytical solutions for multi-dimensional problems. The heat transfer model for the PCM-metal foams composite was established based on the concept of average volume of the composite materials. The internal convection was ignored due to the relatively small thermal resistance caused by the buoyancy force inside the PCM capsule. The case study of paraffin showed that the effective thermal diffusivity and effective thermal conductivity were improved by more than 21 times due to the embedding of Al foams in the PCM. As a result, the temperature of the PCM-metal foams composite became more uniform, while the cold discharge rate was improved by approximately 8 times. The comparative study of different PCMs with/ without Al foams indicated the value of effective thermal diffusivity in weighing the charge/ discharge rate in LHTES systems.

Keywords: Charge/discharge rate; PCM-metal foams composite; effective thermal diffusivity; LHTES.

1. Introduction

Latent heat thermal energy storage (LHTES) has a high energy storage density and a small variation of operating temperature due to the use of phase change materials (PCM) as the storage media [1]. However, one of the major disadvantages of the technology is that the energy storage material has a small thermal conductivity [2-5]. For example, the thermal conductivities of commonly used PCM are approximately 0.1~0.2 W/(m.K) for paraffin, 0.4~0.6 W/(m.K) for salt and salt hydrates and 0.3~0.5 W/(m.K) for fatty acids. This leads to a low charge/ discharge rate of the LHTES module. Moreover, PCMs used as the energy storage media are encapsulated in a shell that is fabricated in different shapes in real life. During the phase change process, the solid- liquid interface moves away from the heat transfer surface. Due to the volume change of the PCM during phase change, the thermal

resistance between the PCM and the heat transfer fluid (HTF) increases, leading to a further reduced charge/ discharge rate of the system. Therefore, improvement of charging/ discharging behaviour is highly required for most latent heat thermal energy applications.

In principle, feasible approaches for improving charge/ discharge rate of PCM based energy storage system include increasing thermal conductivity of PCM, extending heat transfer area and enhancing convective heat transfer between PCM and HTF. However, the most widely used techniques for heat transfer enhancement rely on the improvement of the effective thermal conductivity of the materials [6]. These mainly include the application of embedded fins into PCM [7-9] and impregnation of metal matrix using materials with high thermal conductivity, e.g. carbon fiber, brushes [10-12] and multitubes [13-15]. As a consequence, the effective thermal conductivity of the PCM composite is largely improved, indicating an increased moving speed of the solid/ liquid interface during the conduction-dominated regime of the PCM. However, due to the lower porosity and lower permeability of the fins or metal matrixes, the convective heat transfer was severely constrained [16].

As a complex structures with high thermal conductivity, permeability and specific surface area (due to high porosity and pore density), open-cell metal foams is regarded as a perfect structure to be embedded in PCMs for the improvement of charge/ discharge rate of LHTES systems. Numerous peer studies have focused on the charge/ discharge behaviours of different PCM-metal foams composites. Examples of PCM composites include metal foams impregnated with water [17], salt hydrate [18], organic PCMs [19, 20] and paraffin [21-22]. The feasibility of the concept of using PCM-metal foams composite for high temperature thermal energy storage application were experimentally investigated in [23-25]. It was reported that the charging and discharging period of the system was largely shortened due to the significantly enhanced thermal conductivity of the materials. Thermal analysis of solid/liquid phase change heat transfer in the PCM composite was carried out in [25-26].

However, their models were established based on heat conduction, without consideration of natural convection during the phase change process. Subsequently, a two-dimensional model considering the coupling effect of heat conduction and natural convection were established in [27]. It was found that the effect of natural convection was limited owing to the embedding of metal foams in PCM modules. In most of the aforementioned papers, the effective thermal conductivity was reckoned as the significant factor that contributed to the charge/ discharge rate improvement of PCM based thermal energy storage system.

The present study investigates the cold charging/ discharging behaviour of a PCM-metal foams composite in a cold energy storage (CES) system, in the aim to explore the critical parameters for improving the charge/ discharge rate of the LHTES system.

2. Product solution method

Since real-life PCM capsule has definite storage volume, the heat transfer model for the PCM-metal foams composite was established in multi dimensions. To overcome the difficulty in solving the complicated equations, product solution method was adopted for transforming multi-dimensional physical problems into two or three one-dimensional problems. The synthesis of the analytical solution include the geometry combination and the solution combination, which are specifically illustrated in the following sections.

2.1 Geometry combination

For PCM capsule in the shape of regular prism, it can be regarded as an infinite long prism perpendicularly intersected by an infinite plate. An infinite long rectangular cylinder with a sectional dimension of $2\delta_1 \times 2\delta_2$ can be regarded as the result of the intersection of two infinite plates with a thickness of $2\delta_1$, $2\delta_2$, respectively, as shown in Figure 1. In this case, two-dimensional problem can be transformed as two one-dimensional problems.

Similarly, a short cylinder can be regarded as the intersection of an infinite plate of 2δ thick and an infinite long cylinder with a radius of R, as shown in Figure 2. In this case, three-dimensional problem is transformed as the combination of the one-dimensional problem in the infinite plate and the two-dimensional problem in the infinite long cylinder.

2.2 Solution combination

Based on the geometry combination, two or three dimensional thermal conduction solution in typical geometries can be calculated by multiplying two or three one-dimensional solutions. For example, the short regular prism in Figure 1 (b) has a combined solution as formulated in Eq. (1):

$$\Theta(x,y,\tau)=\Theta_x(x,\tau)\cdot\Theta_y(y,\tau) \qquad (1)$$

Where $\Theta(x,y,\tau)$ is the solution of two dimensional problem for the short regular prism; $\Theta_x(x,\tau)$, $\Theta_y(y,\tau)$ are the solution of infinite plate (x direction, Figure 1a) and the solution of infinite long prism (r direction, Figure 1b), respectively.

The verification of the combined solution can be found in the Appendix. The basic idea is to prove the structure of the combined solution in the condition that $\Theta_x(x,\tau)$, $\Theta_y(y,\tau)$ are the solutions of the infinite plate and the infinite long prism, respectively. Both governing equations and definite conditions (including the initial conditions and boundary conditions) are analyzed. It is proved that solution of the two-dimensional problem can be written as combination of the two one-dimensional solutions. Therefore, the product solution method is advantageous in simplifying the analysis for obtaining the solutions of multi-dimensional problems.

The product solution method can be used in the following definite conditions: (1) The third-class thermal boundary conditions; (2) Initial temperature remains constant. However, it

is pointed out that it also can be applied under the first-class thermal boundary conditions when temperature on the boundary is a constant value.

3. Physical and mathematical models

3.1 Two dimensional heat transfer model

Although the storage volume of PCM is slightly reduced due to the embedding of metal foams in the PCM, the effective thermal conductivity of the composite material increases significantly. This leads to an improved charge/ discharge rate of the LHTES system.

For establishing the heat transfer model for charging/ discharging behaviour in the composite materials in capsules, the characteristics of heat transfer performance were explicitly demonstrated. Forced convection caused by fluid discharging on the outside wall of the PCM capsule was taken into account, which was shown in the boundary conditions. However, in charging/ discharging processes, convection between the liquid PCM and metal foams was not considered. This is because the thermal resistance of thermal conduction is much smaller than that of convection caused by buoyancy force inside the composite materials. As a consequence, single-equation model was used for describing the heat transfer characteristics in the PCM-metal foams composite. The energy equation for a cylinder-shaped PCM module charged/ discharged by fluid flowing outside is written as in Eq.(2):

$$(\rho \cdot Cp)_m \cdot \frac{\partial T}{\partial t} = k_m \cdot (\frac{\partial^2 T}{\partial x^2} + \frac{1}{r} \cdot \frac{\partial T}{\partial r} + \frac{\partial^2 T}{\partial r^2}) \qquad (2)$$

Where k_m represents the effective thermal conductivity of the PCM module. Three-dimensional cellular morphology model for calculating effective thermal conductivity in metal foams can be found in [16]. $(\rho \cdot Cp)_m$ is the averaged energy storage density per unit temperature change of the composite materials, which can be calculated as:

$$(\rho \cdot Cp)_m = (1-\varepsilon) \cdot \rho_s \cdot Cp_s + \varepsilon \cdot \rho_f \cdot Cp_f \qquad (3)$$

Where ε is porosity of metal foams, usually in the range of $0.85 \sim 0.98$; ρ_s, ρ_f are density of metallic fibre and PCM, respectively; Cp_s, Cp_f are heat capacity of metal foams and PCM, respectively.

On the boundary of the PCM capsule, the third-class thermal boundary condition was assumed (with a convective heat transfer coefficient h). Energy balance by forced convection and thermal conduction within the PCM-metal foams composite was established. However, due to the multi-dimensional thermal conduction within the PCM capsule, the temperature correlation is complex. Instead, analytical model based on the product solution method was adopted for the thermal analysis.

3.2 Analytical model

As discussed above, a short cylinder of 2δ long with a radius of R can be intersected by an infinite plate of 2δ thick and an infinite long cylinder with a radius of R, as shown in Figure 2. For the infinite plate, thermal conduction with forced convection on the boundary has the analytical solution that can be expressed as in Eq. (4):

$$\theta_x(x,t) = \theta_{xo} \cdot A_x \cdot e^{-\mu_{1x}^2 \cdot Fo_x} \cdot \cos(\mu_{1x} \cdot \frac{x}{\delta}) \qquad (4)$$

Where θ_{xo} is the initial excess temperature of the plate; $\theta_x(x,t)$ represents the excess temperature of the plate at different position and time; Fo_x is Fourier number in the x direction, defined as:

$$Fo_x = \frac{k_m}{(\rho \cdot Cp)_m} \cdot \frac{\tau}{\delta^2} \qquad (5)$$

A_x and μ_{1x} are two coefficients, calculated as:

$$A_x = 1.0101 + 0.2575 \cdot (1 - e^{-0.4271 \cdot Bi_x}) \qquad (6)$$

$$\mu_{1x} = (0.4022 + \frac{0.9188}{Bi_x})^{-1/2} \quad (7)$$

Where Bi_x denotes Biot number in the x direction, defined as:

$$Bi_x = \frac{h \cdot \delta}{k_m} \quad (8)$$

While for the infinite long cylinder, since the uniform heat transfer surrounds the cylinder-shaped capsule, the physical problem can be simplified as one-dimensional thermal conduction coupled with the third-class thermal boundary condition. The analytical solution can be expressed as in Eq. (9):

$$\theta_r(r,t) = \theta_{ro} \cdot A_r \cdot e^{-\mu_{1r}^2 \cdot Fo_r} \cdot J_0(\mu_{1r} \cdot \frac{r}{R}) \quad (9)$$

Where θ_{ro} is the initial excess temperature of the infinite long cylinder; $\theta_r(r,t)$ represents the excess temperature of the infinite long cylinder along the radius direction at different time; Fo_r is Fourier number in the r direction, defined as:

$$Fo_x = \frac{k_m}{(\rho \cdot Cp)_m} \cdot \frac{4\tau}{R^2} \quad (10)$$

The Bessel function $J_0(x)$ is approximately calculated as:

$$J_0(x) = 0.9967 + 0.0354 \cdot x - 0.3259 \cdot x^2 + 0.0577 \cdot x^3 \quad (11)$$

Where x is substituted by $\mu_{1r} \cdot \frac{r}{R}$ as in Eq. (9).

The coefficients A_r, μ_{1r} can be obtained by Eq.(12)~(13):

$$A_r = 1.0042 + 0.5877 \cdot (1 - e^{-0.4038 \cdot Bi_r}) \quad (12)$$

$$\mu_{1r} = (0.1700 + \frac{0.4349}{Bi_r})^{-1/2} \quad (13)$$

Where Bi_r represents the Biot number for the infinite long cylinder, as expressed in Eq.(14):

$$Bi_r = \frac{h \cdot R}{2k_m} \qquad (14)$$

Therefore, in terms of the product solution method, the temperature distribution of the PCM-metal foams composite can be written as the product of the solutions for the infinite big plate and the infinite long cylinder, as formulated in Eq. (15):

$$\theta(x,r,t) = \frac{\theta_x(x,t) \cdot \theta_r(r,t)}{\theta_0} \qquad (15)$$

In which θ_0 is the initial excess temperature of the PCM module before the charging/ discharging processes.

4. A case study for the PCM-metal foams composite

A case study was carried out to investigate the enhancement of the cold discharging rate by embedding high porosity metal foams in PCM of paraffin. The value of the effective thermal diffusivity and thermal conductivity of the composite materials was proven.

4.1 Sample problem description

A paraffin module was regarded as the PCM in the sample problem and shaped as a short cylinder of L long ($L = 0.6m$) with a radius of R ($R = 0.2m$). Open-cell metal foams with a porosity of 0.8 ($\varepsilon = 0.8$) and a pore density of 20 ($PPI = 20$) was embedded in the paraffin module to form the PCM-metal foams composite. Volume-average method was used to evaluate the thermal physical parameters of the composite materials.

In the discharging process, air with a constant temperature of 20 ^oC flows across the PCM-metal foams composite. The initial temperature of the PCM composite is -30 ^oC, which is 50 ^oC lower than the air temperature. The convective heat transfer coefficient h was supposed to be 120 $W/m^2 \cdot K$. In the cold discharging process, temperature of the PCM-

metal foams composite increased gradually until the energy balance was achieved. The specific parameters of the metal foams, paraffin and air were listed in Table 1.

The geometric origin of the PCM-metal foams composite was defined as the central point of the PCM module, as shown in Figure 3. Therefore, the boundary conditions on the lines OA and OC fulfils the symmetric temperature condition due to the symmetry of the geometry. While temperature on the boundaries of AB and BC was set under the third-class thermal boundary condition. The initial conditions and boundary conditions of the cold energy extraction for the PCM-metal foams composite materials were summarized in Table 2.

4.2 Temperature distribution in the cold discharging process

Based on the above conditions, the temperature distribution of the cylinder-shaped PCM-metal foams composite was obtained. The radial and axial distributions of excess temperature at different locations were demonstrated in Figure 4 and Figure 5, respectively. With time going, cold discharging rate became smaller due to the reduced temperature difference between the PCM module and the flowing air. After 2400 s, the excess temperature was less than 5 ^{o}C , indicating that more than 90% of the cold energy had been extracted by the convection with the air flow. Compared with the temperature on the boundaries of the PCM module, it was found that the average excess temperature on the right boundary ($x/\delta = 1.0$) was lower that on the upper boundary ($r/R = 1.0$).This is due to the smaller thermal resistance in the radial direction, which is caused by the smaller radius ($R = 0.2$) than half length of the cylinder ($\frac{1}{2}L = 0.3$).

The time-dependent temperature distribution on typical points of the PCM module was shown in Figure 6. It was clear that point O (0,0) had the highest excess temperature, while point B (1,1) had the lowest. It was noted that excess temperature at point C (1,0) was smaller than that at point A (0,1). This indicated a larger cold discharge rate along the radial direction.

4.3 Effective thermal diffusivity and thermal conductivity

For demonstrating the effect of metal foams on enhancement of the cold discharging rate, temperature distributions of PCM modules with and without metal foams embedding were compared. As shown in Figure 7, the excess temperature distribution of the PCM without metal foams along the radial direction was much higher than that of PCM module embedded with metal foams. This indicated that the cold discharging rate of the PCM-metal foams composite was largely improved due to the use of metal foams. At the point of (0.5,0), temperatures of the two different PCM modules were compared. Without metal foams, the excess temperature of the PCM module was reduced to 35 ^{o}C after 4800 s; with metal foams, it took 600 s to reach the same temperature level. From this point of view, the cold discharge rate was improved by approximately 8 times. In addition, the temperature of the PCM module became more uniform due to the embedding of the metal foams.

The cold discharge rate of the PCM-metal foams composite is enhanced due to the improvement of the effective thermal conductivity k_m. Based on the formulas in [16], the effective thermal conductivity of the PCM-metal foams composite can be calculated, as shown in Eq. (16):

$$k_m = \frac{\sqrt{2}}{2(R_A + R_B + R_C + R_D)} \qquad (16a)$$

$$R_A = \frac{4\lambda}{(2e^2 + \pi\lambda(1-e))k_s + (4-2e^2-\pi\lambda(1-e))k_f} \quad (16b)$$

$$R_B = \frac{(e-2\lambda)^2}{(e-2\lambda)e^2k_s + (2e-4\lambda-(e-2\lambda)e^2)k_f} \quad (16c)$$

$$R_C = \frac{(\sqrt{2}-2e)^2}{2\pi\lambda^2(1-2e\sqrt{2})k_s + (2\sqrt{2}-2e--\pi\lambda^2(1-2e\sqrt{2}))k_f} \quad (16d)$$

$$R_D = \frac{2e}{e^2k_s + (2e-4\lambda-(4-e^2)k_f} \quad (16e)$$

$$\lambda = \sqrt{\frac{\sqrt{2}(2-(5/8)e^3\sqrt{2}-2\varepsilon}{\pi(3-4e\sqrt{2}-e)}},\ e = 0.339 \quad (16f)$$

In which k_s, k_f represent the thermal conductivity of metal foams and PCM, respectively. It is seen that the effective thermal conductivity of the composite materials is determined by k_s, k_f, three dimensional structure and porosity of the open-cell metal foams.

In the case study, Al foams was embedded in paraffin materials. The thermal conductivity of Al foams (k_s) and paraffin (k_f) is 200 $W/(m\cdot K)$ and 0.558 $W/(m\cdot K)$, respectively. Therefore, the effective thermal conductivity of the PCM-metal foams composite was calculated as 12.6 $W/(m\cdot K)$ in terms of the above model, which was as 22.6 times big as that of paraffin. This can explain the enhancement of charge/ discharge rate in a LHTES system. However, effective thermal conductivity is not the only factor that affects charge/ discharge rate of the PCM composite. As can be seen from Eq. (2), effective thermal diffusivity ($\frac{k_m}{(\rho Cp)_m}$) is a critical property that need to be considered.

Temperature distributions of different PCMs (Paraffin and $NaCO_3$) with and without metal foams were compared in Figure 8 and Figure 9, respectively. Without metal foams embedded in PCM, cold discharging rate of $NaCO_3$ module was larger than that of the paraffin module,

which was due to the larger thermal conductivity of $NaCO_3$, as shown in Table 3. Therefore, without embedding Al foams, it is sensible to use $NaCO_3$ as the PCM for achieving an improved charge/ discharge rate.

However, by embedding Al foams in the PCMs, it was seen in Figure 9 that the excess temperature of paraffin-Al foams composite was smaller than $NaCO_3$–Al foams composite, indicating the former had bigger cold discharging rate under the same conditions. This is because paraffin-Al foams composite has the effective thermal diffusivity of $5.763\times10^{-6} m^2/s$, which is 42.5% higher than the value of the $NaCO_3$ –Al foams composite.

The calculated effective thermal conductivity and thermal diffusivity for single paraffin, single $NaCO_3$, paraffin-Al foams composite and $NaCO_3$–Al foams composite were shown in Table 3. The paraffin-Al foams composite had lower effective thermal conductivity but higher effective thermal diffusivity than those of $NaCO_3$–Al foams composite. Since paraffin-Al foams composite had lower excess temperature distribution under the same conditions, it was concluded that effective thermal diffusivity had more significant value in weighing the enhancement of charge/ discharge rate of LHTES systems.

5. Further discussions on real-life featured model

For the above simplified heat transfer model, the real-life open-cell metal foams was not considered. In reality, the solid matrix of metal foams has a three dimensional and heterogeneous interior microstructures, leading to difficulty in capturing the heat transfer features with high accuracy.

The general solution regarding the heterogeneous nature of the open-cell metal foams is the use of volume-average method. The typical diagram of a porous media was shown in Figure 10. The controlled volume V is composed by both α phase (solid matrix) and β

phase (fluid region). The volume for solid matrix and fluid region is written as V_α and V_β, respectively. The microscopic fluid flow in the porous media is significant and can be related to macroscopic physical quantities in a small volume. For example, the averaged value of PCM temperature T_{PCM} can be expressed as:

$$T_{PCM} = <T_\beta> = \frac{1}{V}\int_{V_\beta} T_\beta \cdot dV \qquad (17)$$

In which $<T_\beta>$ represents the average kinetic power of PCM molecular in β phase.

In terms of the volume-average method, the detailed information within a controlled volume is neglected while the influence of heterogeneous interior microstructures can be reflected in geometric properties (i.e. porosity and pore density) of metal foams and effective thermal properties of the PCM-metal foams composite (i.e. thermal conductivity and thermal diffusivity). For more complicated situation such as forced convection in metal foams, more real-life characteristics of open–cell metal foams including flow disturbance by the solid matrix and inertial effect under non-Darcy flow are to be considered.

6. Concluding remarks

PCM-metal foams composite is highly potential to be used as the storage medium in LHTES system for achieving an improved charge/ discharge rate. The case study of paraffin with and without Al foams indicated that the temperature distribution within the PCM capsule became more uniform, and the cold discharge rate of the composite materials was enhanced by approximately 8 times due to the embedding of Al foams in the paraffin material.

The general explanation is the improved effective thermal conductivity of the PCM-metal foams composite. However, the comparative investigation with different PCMs embedded

with/ without Al foams proved the value of the effective thermal diffusivity as the key criteria in weighing the enhancement of charge/ discharge rate of LHTES systems.

Although the present analytical study was based on the volume-average method, the influence of heterogeneous nature of the open-cell metal foams was actually considered, which was reflected in average geometric properties of metal foams and effective thermal properties of the PCM-metal foams composite.

Appendix

The following part is the verification of Eq. (1). The computational domain of the infinite long rectangular cylinder is shown in Figure 3. Due to the symmetry of the geometry, section O-A-B-C is considered.

The governing equation and the definite conditions are shown in Eq. (A.1) ~ (A.4):

$$\frac{\partial \Theta}{\partial \tau} = a \cdot \left(\frac{\partial^2 \Theta}{\partial x^2} + \frac{\partial^2 \Theta}{\partial y^2}\right) \qquad \text{(A.1)}$$

$$\Theta(x, y, 0) = 1 \qquad \text{(A.2)}$$

$$\Theta(\delta_1, y, \tau) + \frac{\lambda}{h} \cdot \frac{\partial \Theta(x, y, \tau)}{\partial x}\Big|_{x=\delta_1} = 0 \qquad \text{(A.3a)}$$

$$\Theta(x, \delta_2, \tau) + \frac{\lambda}{h} \cdot \frac{\partial \Theta(x, y, \tau)}{\partial y}\Big|_{y=\delta_2} = 0 \qquad \text{(A.3b)}$$

$$\frac{\partial \Theta(x, y, \tau)}{\partial x}\Big|_{x=0} = 0 \qquad \text{(A.4a)}$$

$$\frac{\partial \Theta(x, y, \tau)}{\partial y}\Big|_{y=0} = 0 \qquad \text{(A.4b)}$$

Where $\Theta(x, y, \tau)$ is the dimensionless excess temperature, which is defined as follows:

$$\Theta = \frac{T(x, y, \tau) - T_\infty}{T_0 - T_\infty} = \frac{\theta}{\theta_0} \qquad \text{(A.5)}$$

For one dimensional problem for infinite plate (seen Figure 1 a), $\Theta_x(x,\tau)$ is the solution of:

$$\frac{\partial \Theta_x}{\partial \tau} = a \cdot \frac{\partial^2 \Theta_x}{\partial x^2} \qquad \text{(A.6)}$$

$$\Theta_x(x,0) = 1 \qquad \text{(A.7)}$$

$$\Theta_x(\delta_1,\tau) + \frac{\lambda}{h} \cdot \frac{\partial \Theta_x(x,\tau)}{\partial x}\Big|_{x=\delta_1} = 0 \qquad \text{(A.8)}$$

$$\frac{\partial \Theta_x(x,\tau)}{\partial x}\Big|_{x=0} = 0 \qquad \text{(A.9)}$$

For one dimensional problem for infinite long rectangular cylinder (seen Figure 1 b), $\Theta_y(y,\tau)$ is determined by:

$$\frac{\partial \Theta_y}{\partial \tau} = a \cdot \frac{\partial^2 \Theta_y}{\partial y^2} \qquad \text{(A.10)}$$

$$\Theta_y(y,0) = 1 \qquad \text{(A.11)}$$

$$\Theta_y(\delta_2,\tau) + \frac{\lambda}{h} \cdot \frac{\partial \Theta_y(y,\tau)}{\partial y}\Big|_{y=\delta_2} = 0 \qquad \text{(A.12)}$$

$$\frac{\partial \Theta_y(y,\tau)}{\partial y}\Big|_{y=0} = 0 \qquad \text{(A.13)}$$

For verifying Eq. (1) in the 'Product solution method' section, both of the governing equation Eq. (A.1) and the definite conditions Eq. (A.2) ~ (A.4) need to be verified.

Firstly, for the governing equation Eq. (A.1), the left term and right term can be written as:

$$\frac{\partial \Theta}{\partial \tau} = \frac{\partial (\Theta_x \cdot \Theta_y)}{\partial \tau} = \Theta_x \cdot \frac{\partial \Theta_y}{\partial t} + \Theta_y \cdot \frac{\partial \Theta_x}{\partial t} \quad \text{(Left term)} \qquad \text{(A.14a)}$$

$$a \cdot \left(\frac{\partial^2 \Theta}{\partial x^2} + \frac{\partial^2 \Theta}{\partial y^2}\right) = a \cdot \left(\Theta_y \cdot \frac{\partial^2 \Theta_x}{\partial x^2} + \Theta_x \cdot \frac{\partial^2 \Theta_y}{\partial x^2}\right) \quad \text{(Right term)} \qquad \text{(A.14b)}$$

Consequently, the difference of left and right terms is:

$$\Theta_x \cdot \frac{\partial \Theta_y}{\partial t} + \Theta_y \cdot \frac{\partial \Theta_x}{\partial t} - a \cdot (\Theta_y \cdot \frac{\partial^2 \Theta_x}{\partial x^2} + \Theta_x \cdot \frac{\partial^2 \Theta_y}{\partial x^2}) = \Theta_y \cdot (\frac{\partial \Theta_x}{\partial \tau} - a \cdot \frac{\partial^2 \Theta}{\partial x^2}) + \Theta_x \cdot (\frac{\partial \Theta_y}{\partial \tau} - a \cdot \frac{\partial^2 \Theta_y}{\partial y^2}) \quad \text{(A.14c)}$$

Secondly, definite conditions need to be fulfilled. Since the governing equation is verified, the initial condition of Eq.(A.2) becomes:

$$\Theta(x, y, 0) = \Theta(x, 0) \cdot \Theta(y, 0) = 1 \times 1 = 1 \qquad \text{(A.15)}$$

While for the boundary conditions as expressed in Eq. (A.3a) and Eq. (A.4a), we have:

$$\Theta_x(\delta_1, \tau) \cdot \Theta_y(y, \tau) + \Theta_y(y, \tau) \cdot \frac{\lambda}{h} \cdot \frac{\partial \Theta_x(x, \tau)}{\partial x}\Big|_{x=\delta_1} = \Theta_y(y, \tau) \cdot [\Theta_x(\delta_1, \tau) + \frac{\lambda}{h} \cdot \frac{\partial \Theta_x(x, \tau)}{\partial x}\Big|_{x=\delta_1}] = 0 \quad \text{(A.16)}$$

$$\frac{\partial \Theta(x, y, \tau)}{\partial x}\Big|_{x=0} = \frac{\partial \Theta_x(x, \tau)}{\partial x}\Big|_{x=0} \cdot \Theta_y(y, \tau) = 0 \cdot \Theta_y(y, \tau) = 0 \qquad \text{(A.17)}$$

Similarly, Eq. (A.3b) and Eq. (A.4b) can be validated.

From Eq. (A.14c), Eq. (A.15)~ (A.17), it is concluded that, in the condition that $\Theta_x(x, \tau)$, $\Theta_y(y, \tau)$ are the solutions of Eq.(A.6) and Eq.(A.10), solution of governing equation Eq. (A.1) can be written as combination of the two one-dimensional solutions, as shown in Eq. (1) in the 'Product solution method 'section.

Acknowledgement

We would like to acknowledge EPSRC Grants (EP/L014211/1, EP/K002252/1 and EP/L019469/1) for financial support.

References

[1] Niu F X, Ni L, Yao Y, Yu Y B, Li H R. Performance and thermal charging/ discharging features of a phase change material assisted heat pump system in heating mode. Appl. Therm. Eng. 2013; 58: 536-41.

[2] Guichard S, Miranville F, Bigot D, Boyer H. A thermal model for phase change materials in a building roof for a tropical and humid climate: model description and elements of validation. Energy Build. 2014; 70: 71-80.

[3] Agyenim F. The use of enhanced heat transfer phase change materials (PCM) to improve the coefficient of performance (COP) of solar powered LiBr/ H_2O absorption cooling system. Renew. Energy 2016; 87: 229-39.

[4] Ermis K, Erek A, Dincer I. Heat transfer analysis of phase change process in a finned-tube thermal energy storage system using artificial neural network. Int. J. Heat Mass Transf. 2007; 50: 3163-75.

[5] Ismail K A R., Alves C L F, Modesto M S. Numerical and experimental study on the solidification of PCM around a vertical axially finned isothermal cylinder. Appl. Therm. Eng. 2001; 21: 53-77.

[6] Du Y P. Cold energy storage: fundamentals and applications. PhD thesis, 2014.

[7] Agyenim F, Eames P, Smyth M. A comparison of heat transfer enhancement in a medium temperature thermal energy storage heat exchanger using fins, Sol. Energy 2009; 83: 1509-20.

[8] Horbaniuc B, Dumitrascu G, Popescu A. Mathematical models for the study of solidification within a longitudinally finned heat pipe latent heat thermal storage. Energy Convers. Manag. 1999; 40: 1765-74.

[9] Zhang Y, Faghri A. Heat transfer enhancement in latent heat thermal energy storage system by using longitudinally finned tube. Int. J. Heat Mass Transf. 1996; 39: 3165-73.

[10] Wi S, Seo J, Jeong S, Chang S J, Kang Y, Kim S. Thermal properties of shape stabilized phase change materials using fatty acid ester and exfoliated graphite nanoplatelets for saving energy in buildings. Sol. Energy Mater. Sol. Cells 2015; 143: 168-73.

[11] Wu W, Zhang G, Ke X, Yang X, Wang Z, Liu C. Preparation and thermal conductivity enhancement of composite phase change materials for electronic thermal management. Energy Convers. Manag. 2015; 101: 278-84.

[12] Ling Z, Chen J, Xu T, Fang X, Gao X, Zhang Z. Thermal conductivity of an organic phase change material/expanded graphite composite across the phase change temperature range and a novel thermal conductivity model. Energy Convers. Manag. 2015; 102: 202-208.

[13] Agyenim F, Hewitt N, Eames P, Smyth M. A review of materials, heat transfer and phase change problem formulation for latent heat thermal energy storage systems (LHTESS). Renew. Sustainable Energy Rev. 2010; 14: 615 – 28.

[14] Esen M, Ayhan T. Development of a model compatible with solar assisted cylindrical energy storage tank and variation of stored energy with time for different phase change materials. Energy Convers. Manag. 1996; 37: 1775-85.

[15] Agyenim F, Eames P, Smyth M. Heat transfer enhancement in medium temperature thermal energy storage system using a multitube heat transfer array. Renew. Energy 2010; 35: 198-207.

[16] Boomsma K, Poulikakos D. On the effective thermal conductivity of a three dimensionally structured fluid-saturated metal foam. Int. J. Heat Mass Transf. 2001; 44: 827 –36.

[17] Chi, P, Xie Y, Yu J, Yang X. Experiment and analysis for cold charging process of new energy storage device. Journal of Beijing University of Aeronautics and Astronautics 2011; 37: 1070-75.

[18] Sheng Q, Xing Y, Wang Z. Preparation and performance analysis of metal foam composite phase change material. Journal of Chemical Industry and Engineering 2013; 64: 3565-70.

[19] Jiang J H, Zhu Y Y, Ma A B, Yang D H, Lu F M., Chen J Q, Shi J, Song, D. Preparation and performances of bulk porous Al foams impregnated with phase-change-materials for thermal storage. Progress in Natural Science: Materials International 2012; 22: 440- 44.

[20] Zhang T, Yu J. Experiment of solid-liquid phase change in copper foam. Journal of Beijing University of Aeronautics and Astronautics 2007; 33: 1021-24.

[21] Cui H T. Experimental investigation on the heat charging process by paraffin filled with high porosity copper foam. Appl. Therm. Eng. 2012; 39: 26-28.

[22] Xiao X, Zhang P, Li M. Preparation and thermal characterization of paraffin/metal foam composite phase change material. Appl. Energy 2013; 112: 1357-66.

[23] Zhao C Y, Wu Z G. Heat transfer enhancement of high temperature thermal energy storage using metal foams and expanded graphite. Sol. Energy Mater. Sol. Cells 2011; 95: 636-43.

[24] Zhou D, Zhao C Y. Experimental investigations on heat transfer in phase change materials (PCMs) embedded in porous materials. Appl. Therm. Eng. 2011; 31: 970-77.

[25] Zhao, C Y, Lu, W, Tian Y. Heat transfer enhancement for thermal energy storage using metal foams embedded within phase change materials (PCMs). Solar Energy 2010; 84: 1402-12.

[26] Siahpush A, O'Brien J, Crepeau J. Phase Change Heat Transfer Enhancement Using Copper Porous Foam. J. Heat Transfer 2008;130: 082301-1 to 082301-11.

[27] Tian Y, Zhao C Y. A numerical investigation of heat transfer in phase change materials (PCMs) embedded in porous metals. Energy 2011; 36: 5539-46.

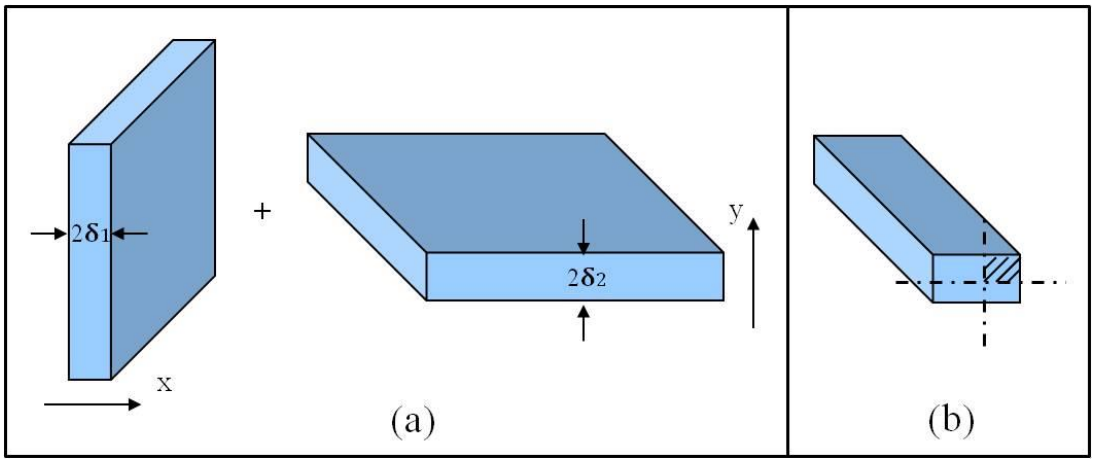

Figure 1. Infinite long rectangular cylinder with a sectional dimension of $2\delta_1 \times 2\delta_2$.

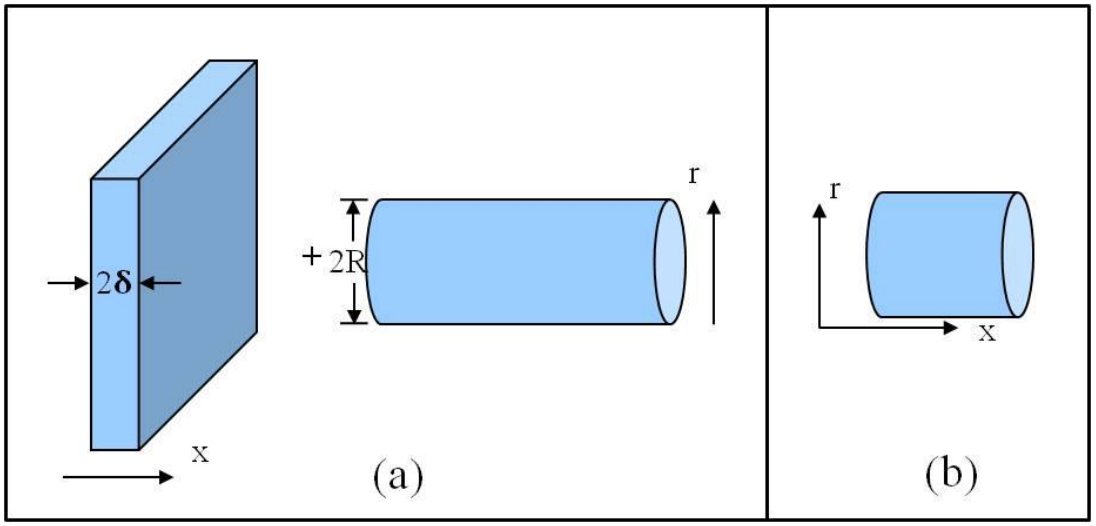

Figure 2. Formation of a short cylinder.

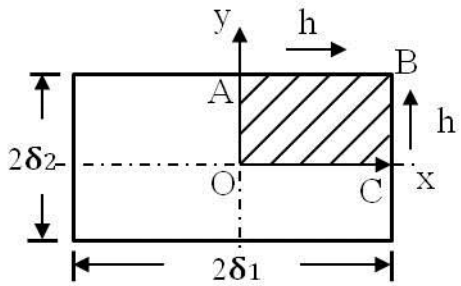

Figure 3. Computational domain of rectangular cylinder.

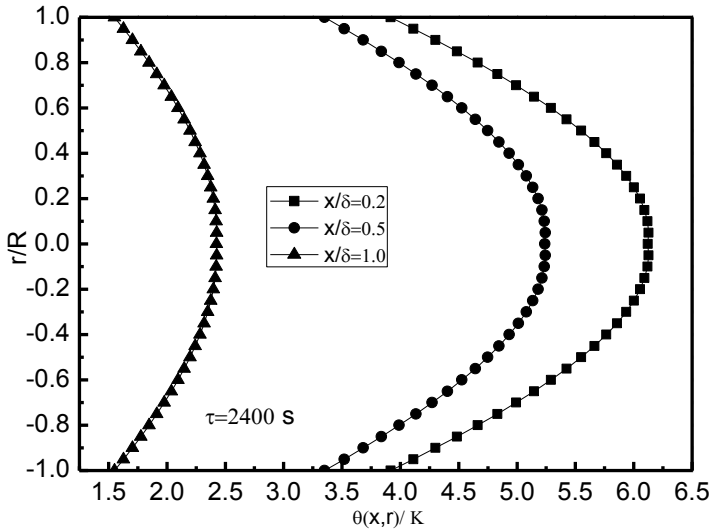

Figure 4. Radial distributions of the excess temperature.

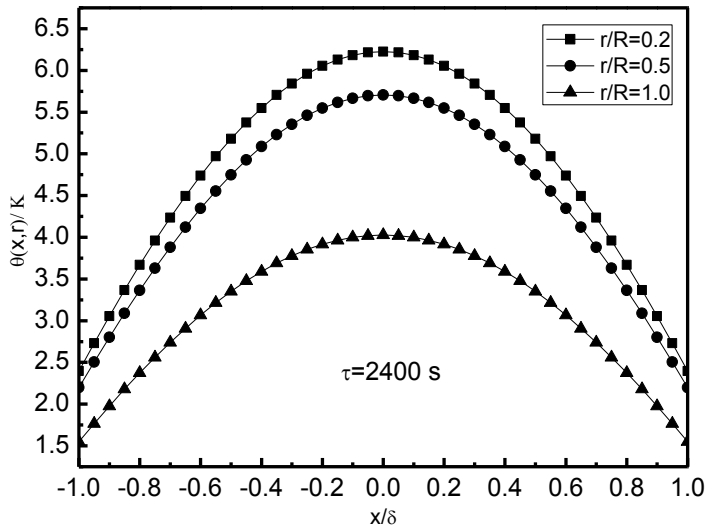

Figure 5. Axial distribution of the excess temperature.

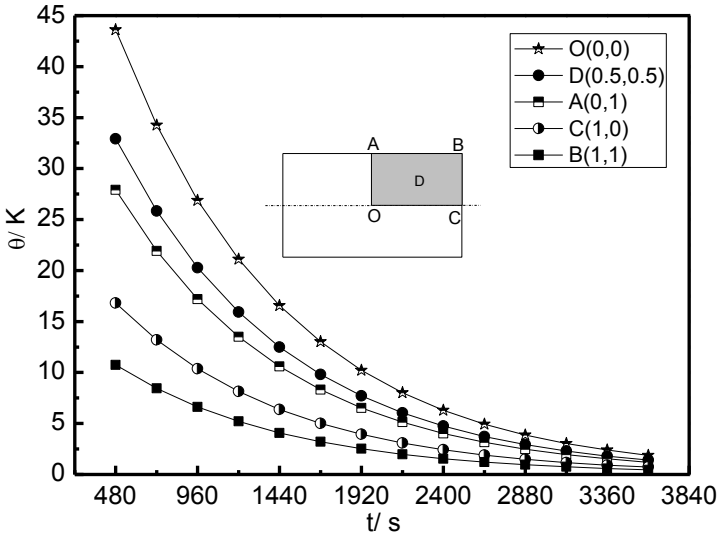

Figure 6. The time-dependent distribution on typical points.

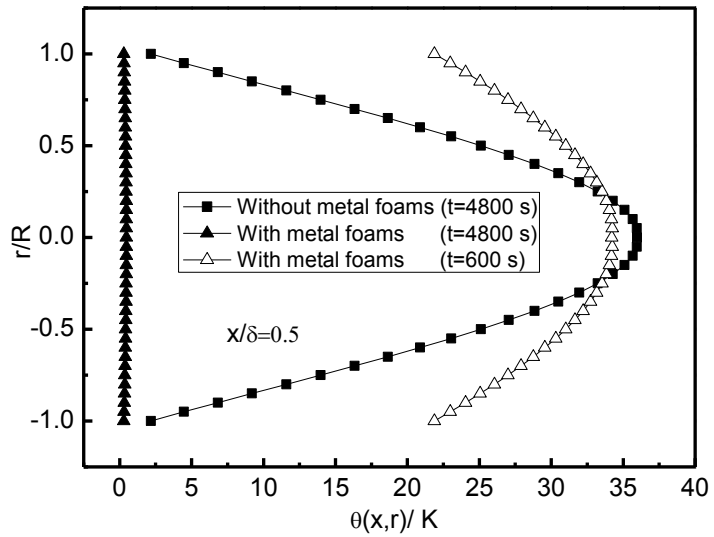

Figure 7. The effect of metal foams on cold discharge rate.

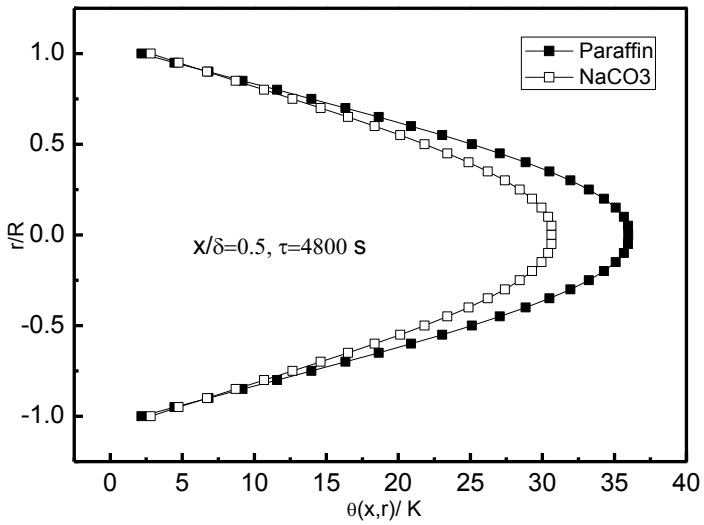

Figure 8. Temperature distributions of different PCM without metal foams.

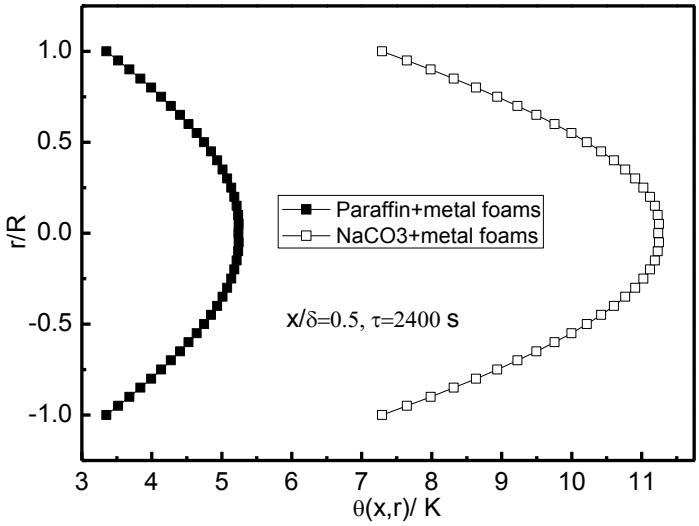

Figure 9. Temperature distributions of different PCMs embedded with metal foams.

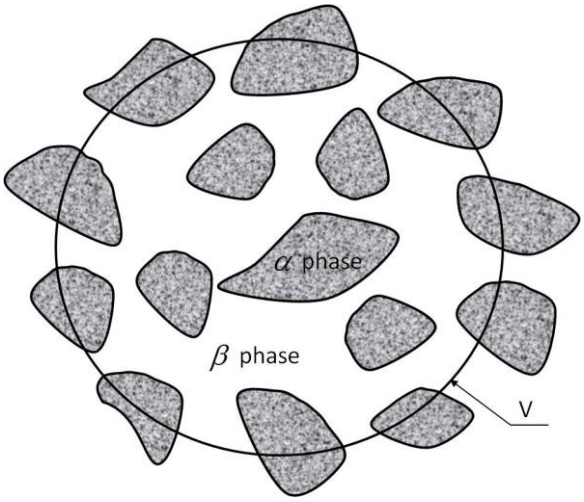

Figure 10. Controlled volume in a typical porous media.

Table 1. Parameters of PCM-metal foams composite in discharging process.

ρ_s kg/m^3	Cp_s $J/(kg\cdot K)$	k_s $W/(m\cdot K)$	ρ_f kg/m^3	Cp_f $J/(kg\cdot K)$	k_f $W/(m\cdot K)$	r kJ/kg	ε	h $W/(m^2\cdot K)$	L m	R m
2500	2000	200	855	2400	0.558	200	0.8	120	0.6	0.2

Table 2. Initial and boundary conditions.

T_{air} ^oC	$T_{PCM,i}$ ^oC	Boundaries of the geometry			
		OA	OC	AB	BC
20	-30	$\frac{\partial T_{PCM}}{\partial x}=0$	$\frac{\partial T_{PCM}}{\partial y}=0$	$h\ W/(m^2\cdot K)$	
				120	

Table 3 Calculated thermal properties of different materials.

Materials	k_m $W/(m\cdot K)$	$(\rho\cdot Cp)_m$ $10^{-6}J/(m^3\cdot K)$	$\frac{k_m}{(\rho\cdot Cp)_m}$ $10^6 m^2/s$	Bi_x	Bi_r	Fo_x	Fo_r
Paraffin	0.558	2.1375	0.261	64.5	21.5	0.384	3.132
$NaCO_3$	0.83	2.4444	0.339	43.4	14.5	0.453	4.077
Paraffin+ Al foams	12.6	2.186	5.763	2.86	0.95	7.69	69.21
$NaCO_3$+Al foams	13.1	3.239	4.044	2.75	0.92	5.39	48.51